International Journal of
INTELLIGENT SYSTEMS AND APPLICATIONS IN ENGINEERING
ISSN:2147-6799 www.ijisae.org Original Research Paper

Brain Tumor Detection using CNN and VGG-16 Model

Amit Sharma[1], Sunny Arora[2]

Submitted: 26/01/2024 **Revised**: 04/03/2024 **Accepted**: 12/03/2024

Abstract: Modern healthcare heavily relies on the timely and precise detection of brain tumors (BT), a critical factor influencing patient outcomes. Uncontrolled proliferation of brain cells can lead to the growth of BT. Common imaging methods, such as MRIs, CT scans, and radiography, are routinely employed to detect and diagnose these tumors. Despite these advanced techniques, the automatic identification of brain tumors in their early stages remains challenging, particularly through MRI scans. While reviewing the conventional approaches in brain tumor identification, several persistent issues were identified. These include a lack of diversity in the images, challenges in feature extraction, and a limited evaluation of extensive multiclass datasets. This study investigates the efficacy of various state-of-the-art ML and DL models, including RF, SVM, KNN, CNN, VGG16, and AlexNet, for brain tumor identification. Python was executed for simulating these models, and their performance is assessed on two extensive databases— BTIS and Glioma. Evaluation is conducted based on three crucial metrics: accuracy, precision, and recall. For maximizing the accuracy of tumor boundary definition and overall algorithmic efficacy, the SS algorithm is introduced. In this study, the CNN algorithm serves as a benchmark for the analysis and to categorize tumorous images, leveraging the efficiency of VGG16 and AlexNet in capturing intricate image features. The outcomes indicate the reliability of these algorithms in accurately diagnosing and localizing brain tumors. The comparative study systematically assesses and illustrates the effectiveness and limitations of these algorithms. Notably, VGG16 demonstrated impressive results with an accuracy of 95.23%, recall of 93.72%, precision of 93.27%, and an F1-Score of 94.22%.

Keywords: *Brain Tumor, CNN, VGG16, Alex Net, RF, SVM, KNN*

1. Introduction

In recent times, digital medicinal pictures are proven invaluable for teaching, research, and diagnosing various disorders. There is a pressing need for a precise and efficient computer-assisted diagnostic system to streamline the generation of medical reports and advance research in medical imaging [1]. The current approach to calculating clinical imaging scans has been time-consuming, error-prone, and ineffective in accurately diagnosing brain tumors (BTs). Despite being the 10th leading cause of death, the existing methods for BT recognition, particularly through MRI, have fallen short in terms of accuracy. Brain tumors pose a significant health risk, and MRI, with its non-invasive and effective components, offers a comprehensive imaging solution for soft tissue [1]. This enables the extraction of information regarding the shape, location, and size of tumors without subjecting patients to high doses of ionizing radiation. Presently, there is a growing emphasis on the automated diagnosis of brain tumors, leading to the creation of numerous comprehensive solutions [2]. The rapid progress in machine learning and image processing has facilitated these advancements in the healthcare sector.

In the current technological era, the most dependable diagnostic method is Magnetic Resonance Imaging (MRI). This approach eliminates the use of ionizing radiation, offering a straightforward way to gather information about the location, dimensions, and composition of human tissues and body components. The resulting scans are both accurate and clear, providing enhanced precision in disease diagnosis and eliminating the need for contrasting empirical techniques. Moreover, Magnetic Resonance Imaging serves as a reliable resource for interference planning and lesion localization [3]. A number of mechanisms are put forward in Brain Tumor Magnetic Resonance Imaging, such as 3D multi-band scanning and chest X-rays. Notably, the three-dimensional multiband MRI proves to be a more practical and informative method for precisely pinpointing lesion locations. This development helps this method capture different compositions in the same tissue.

In today's healthcare landscape, numerous hospitals and websites offer extensive information on a wide array of illnesses. These data sources serve as crucial tools for academics, which facilitate to employ diverse mechanisms to execute different tasks, including evaluating the newly developed algorithms or identifying clinical disorders [4]. MRI stands out as the predominant approach which diagnoses cancer. What sets MRI apart is its unique ability to provide precise details about the dimensions, shapes, and positions of human tissues and organs without subjecting patients to excessive doses of ionizing radiation. The resulting MRI images are highly accurate and sharp. Notably, the significant improvements in MRI's diagnostic

[1]*Department of Computer science and engineering, Guru Kashi University, Talwandi Sabo (151302), Bathinda, Punjab, India*
ORCID ID: 0009-0005-1629-3244
[2] *Department of Computer science and engineering, Guru Kashi University, Talwandi Sabo (151302), Bathinda, Punjab, India*
ORCID ID: 0000-0003-1971-7514
[1]*amit.kaushik333@gmail.com*, [2]*sunnyaro@gmail.com*

capabilities have rendered procedures like thoracotomies and laparotomies unnecessary. Furthermore, MRI serves as a dependable means to detect lesions and plan surgical procedures [3]. MRI employs various techniques, including three-dimensional multi-band imaging and chest X-ray scanning. Particularly noteworthy is the use of 3D multiband MRI, which, unlike 2D imaging, allows for precise localization of lesion regions, providing vital information for doctors. This often-underappreciated innovation in MRI enables the capture of numerous compositions within the same tissue.

To enhance the likelihood of identifying suspicious regions in MR images, picture pre-processing is significant in the analysis process. This stage primarily focuses on refining fine image details and reducing noise in the acquired photos, thereby improving the overall image quality. Medical magnetic resonance images damaged by noise tend to be less precise and reliable [5]. A common type of degradation in magnetic resonance imaging is the presence of a smooth signal intensity variation, known as intensity non-consistency, RF inhomogeneity, or bias field. This variation has the potential to make images less sharp by diminishing high-frequency visual features such as edges and outlines. Various image pre-processing techniques are employed to enhance segmentation and feature identification when utilizing MRI images as input. In this pre-processing step, a variety of filtering techniques are applied to reduce noise in the images. These methods effectively minimize unwanted distortions and enhance specific aspects of the image. Segmentation, in which an image is split into dissimilar sections according to chosen characteristic such as color, texture, or saturation, is executed within this process [6]. The objective of segmentation is to enhance the clarity, expressiveness, and conciseness of the image's description. In terms of isolating feature extraction challenges from the task of automatically detecting lesion borders, some researchers argue that physically detecting edges is preferable to computer-assisted boundary identification. However, in order to create computerized diagnosis systems for brain tumour identification, automated segmentation approaches are essential.

The goal of extracting attributes is that the standard data set is mitigated on the basis of quantifying certain characteristics or properties for differentiating an input from another. Pixels are measured to represent a fragmented object so that numerous attributes are computed in feature extraction [7]. GLCM is a statistical method that turns image data into mathematical form in the texture analysis according to the spatial relation between pixels, allowing the co-occurrence matrix to be computed to characterize the texture's properties. The epithelial image of the skin can be used to determine the contrast, correlation, entropy, uniformity, and energy of different diseases. In the diagnostic system's classification phase, conclusions are drawn from the data collected in previous steps to generate a diagnosis for the input image. The image classification is performed via 2 approaches: the first method assigns a class label of 0 or 1 to the data item depending upon the categorical dissimilarity between 2 categories (melanoma and benign) [8]. The next tactic involves modeling P(y|x), introducing the option of a class subscription in addition to assigning a class label to the data item. Image classification utilizes machine learning models.

In 1992, Vapnik introduced the Support Vector Machine (SVM), an effective machine learning (ML) model designed to address complex physics problems characterized by increased nonlinearity. The SVM algorithm is capable of handling higher-dimensional data and capturing non-linear relationships between input variables and output class labels [9]. To achieve this, kernel functions are employed, aiding in the transformation of input data into a high-dimensional space where linear separation is performed. This approach is robust and flexible enough to address supervised learning (SL), gaining popularity in various applications such as natural language processing (NLP), bioinformatics, image classification, and object detection. The fundamental focus is on obtaining an accurate linear delimitation hyperplane (LDH) by mapping one feature space onto another at higher latitudes using nonlinear transformation [10]. In the extended feature framework, SVM can directly calculate the distance between dissimilar data points, which is handled by the kernel functions. The partitioning of kernel functions into three distinct classes i.e., linear kernel (LK), polynomial kernel (PK), and radial basis kernel (RBK) function is done based on different mapping methodologies.

The Decision Tree (DT) machine learning (ML) algorithm finds widespread use in various applications, such as data classification, solving multi-output problems, handling values and outliers, and more. Notably, this algorithm is quick to visualize and generate since it doesn't rely on pre-existing data-related hypotheses. The Decision Tree (DT) algorithm demonstrates superior efficiency compared to traditional techniques [11]. In this technique, a set of training data is organized into trees with leaves and root nodes. The root serves as the fundamental concept characterizing the research or primary feature of the dataset, determining the starting point for creating the algorithm and its initial event. In this approach, the probabilities are akin to branches emanating from the root, connecting to nodes, and further branching into additional nodes. Each internal node represents a decision about a property, determining how the data should be divided among its child nodes. Additionally, the algorithm incorporates various terms like splitting, pruning, and subtree or branch. These terms indicate the removal of specific nodes during the process [12]. A supervised machine learning (ML) technique that aids in data classification is Random Forest (RF). Specifically designed to handle categorical data during

classification, Random Forest (RF) also addresses continuous data to address regression problems. This algorithm is constructed using a large number of decision trees (DT), each utilized to predict a class. The predictive class of the algorithm is determined by the class with the highest number of predictions [13]. The creation of this algorithm involves distinct steps, and each decision node (DT) within the algorithm is structured in a manner resembling a tree.

A dependable supervised machine learning (ML) technique is the artificial neural network (ANN). This algorithm employs multiple interconnected groups of artificial neurons for computational tasks, utilizing a connectionist approach. ANN finds application in several fields, such as to identify speech, data classification, autism gene detection, and natural language processing (NLP). The conventional algorithm is comprised of three types of nodes: input, hidden, and output [14]. The initial nodes represent explanatory metrics, with variations in their features. The output nodes consist of dependent variables, and their quantity is determined by the selected options. Nodes in the artificial neural network are linked to connections and signals that propagate forward. Information about each link is used to calculate various numerical weights. Each node focuses on adding the value input by the preceding node multiplied by the weight [15]. The signal is then propagated to the next layer using an activation function (AF). Common activation functions include the purlin, tan-sigmoid, and SoftMax. The sigmoid activation function (SAF) is often considered the most efficient. Additionally, this technique comprises various components, including bias, weight initialization, feedforward (FF), backpropagation (BP) for error, and updating weights [16, 17].

All standard paper components have been specified for three reasons: ease of use when formatting individual papers, automatic compliance to electronic requirements that facilitate the concurrent or later production of electronic products, and conformity of style throughout a manuscripts. Margins, column widths, line spacing, and type styles are built-in; examples of the type styles are provided throughout this document and are identified in italic type, within parentheses, following the example. Some components, such as multi-leveled equations, graphics, and tables are not prescribed, although the various table text styles are provided. The formatter will need to create these components, incorporating the applicable criteria that follow.

2. Related Work

D. Rammurthy, et.al (2020) introduced a technique named WHHO-based DeepCNN, utilizing the Whale Harris Hawks Optimization (WHHO) model to identify brain tumors in MRI scans [18]. The images were subsequently categorized based on CA and RST. The proposed method was employed to extract properties from the segments, such as tumor size and LOOP. Diagnosing BTs was facilitated by Deep CNN. WHHO, a hybrid of Whale Optimization Algorithm (WOA) and Harris Hawks Optimization (HHO), demonstrated superior performance, achieving an accuracy of 81.6% compared to other methods, as per the provided data.

E. Dandıl, et.al (2020) introduced a stacking model based on LSTM and Bidirectional LSTM (Bi-LSTM) in order to detect BTs [19]. The study utilized the INTERPRET database, containing MRSSs from both healthy and diseased tissues. In the analysis results, the constructed model had yielded 93.44% accuracy for pseudo brain tumors with glioblastoma, 85.56% for diffuse astrocytomas, and 88.33% for brain tissue that had metastasized to other areas. Additionally, the model demonstrated effective performance in diagnosing pseudo brain tumors.

Shiny et al. (2021) detected pixel shifts (DCNN) and diagnosed brain cancers using a hybrid DL-based approach) [20]. The process consists of four stages: segmentation, feature extraction, input/output, and classification. The DBN is integrated with CNN to make decisions based on an error function. The accuracy of suggested mechanism is 0.957. Overall, the results support the hypothesis that DBN + CNN approach can accurately identify pixel changes and classify brain tumors. The utilization of BirCat algorithms in training the network contributes to its enhanced efficiency.

R. Vankdothu, et.al (2022) introduced an additional automated method for analyzing and categorizing brain tumors [21]. The magnetic resonance imaging (MRI) image underwent pre-processing with an adaptive filter for assessment. Improved K-Means Clustering (IKMC) was applied for segmenting image, and the features were extracted using GLCM. The task to categorize images was accomplished using the Region-based CNN, deep learning (DL) algorithm. The introduced framework was simulated on the Kaggle dataset, and the results indicated its superior effectiveness in diagnosing BT from images, achieving 95.17% accuracy.

Okashi et al. (2022) developed a methodology which diagnosed BT in MRI by incorporating multiple variables with an Adaboost classifier [22]. The initial step involves pre-processing the images to delineate the brain region. Subsequently, it focuses on extracting different texture attributes from each region of the brain image. Following this, the schemes of selecting attributes are applied for recognizing the most significant extracted texture properties. The Adaboost classifier is then trained to categorize each patch as either pathological or normal tissue using these selected feature vectors. The results indicated that using STFA, LBP, and HOG features led to increased detection accuracy, reaching 46.5%, 68.96%, and 87.93%, respectively.

Senan et al. (2022) investigated various studies that integrate classic ML with DL for brain cancer identification [23]. By employing AlexNet and ResNet-18 in conjunction with SVM technique, the categorization and diagnosing of BTs were achieved. Deep learning models, utilizing deep convolutional layers, were employed to extract robust and significant deep features. The process of combining deep and machine learning begins with feature mining, utilizing techniques like AlexNet and ResNet-18. Each method demonstrated excellent results. Notably, the suggested approach was effective to diagnose BT at 95.10% success rate.

Raza et al. (2023) introduced a hybrid architecture called dResU-Net to enhance brain tumor segmentation results, combining the advantages of the deep residual network and the U-Net model [24]. The residual network serves as an encoder for extracting high-level attributes, prior to restructuring them using the U-Net decoder. The model's effectiveness was evaluated using the BraTS 2020 dataset. The proposed dResU-Net model demonstrated promising results, with average dice scores for the tumor core (TC), whole tumor (WT), and enhancing tumor (ET) of 0.8357, 0.8660, and 0.8004, respectively. The external cohort dice scores for TC, WT, and ET were 0.8400, 0.8601, and 0.8221, indicating the model's ability to generalize.

Chang et al. (2023) introduced an effective 3D segmentation model called DPAFNet [25]. DPAFNet utilizes residual connectivity and dual-path convolution to expand the network's size, preventing network degradation. Comparative tests with previous studies on BraTS2018, BraTS2019, and BraTS2020 demonstrate promising results, showing improved precision and Dice scores. Specifically, the proposed DPAFNet achieved Dice scores of 79.5%, 90.0%, and 83.9% for the enhancing tumor, entire tumor, and tumor core, respectively, on BraTS2018. On BraTS2019, Dice scores of 78.2% for the tumor core, 89.0% for the entire tumor, and 81.2% for the enhancing tumor were recorded.

Cao et al. (2023) introduced MBANet, a multi-branch CNN with three-dimensional data processing capabilities [26]. The MBANet BU module begins via optimized shuffle unit. In this BU component, the input channel undergoes division, a convolution operation employing group convolution is performed, and the convolutional channels undergo shuffling using channel shuffle. The MBANet encoder incorporates a novel multi-branch 3D Shuffle Attention (SA) module as its attention layer. Additionally, MBANet's skip connection utilizes a 3D SA module to enhance the resolution of the up-sampled semantic features. In experiments on two BraTS datasets from 2018 and 2019, MBANet demonstrated the ability to achieve Dice scores of 80%, 89%, 86% for the enhancing tumor (ET), whole tumor (WT), and tumor core (TC), respectively, and 78%, 87%, 83% for the corresponding regions on each dataset.

S. Tripathy, et.al (2023) proposed a tumor diagnosis technique based on EfficientNet using transfer learning (TL) [27]. Three frameworks—EfficientNet-B2, EfficientNet-B3, and EfficientNet-B4—were chosen for implementation. The objective of this approach was to enhance both accuracy and efficiency through thresholding. Additional data was introduced to augment the dataset and reduce the number of images. The suggested technique demonstrated superior performance in scaling a picture's depth, width, and resolution at a constant ratio. It effectively expanded the display and captured intricate details. The results indicated that, in comparison to various approaches, the proposed strategy achieved an accuracy of 95%.

3. Materials and Methods

3.1. Datasets

The BRATS and Glioma datasets are executed to compute the efficacy of the presented technique. These datasets are defined comprehensively as:

3.1.1. BRATS Dataset

It is crucial source for storing biomedical pictures within clinical imaging. This dataset is assisted in segmenting and classifying brain tumor. Dissimilar MRI scans of brain related to T1-weighted, T1-weighted contrast-enhanced, T2-weighted, and FLAIR (Fluid-Attenuated Inversion Recovery) images are available in this dataset. In addition, this dataset leads to provide vital explanations or real time segmentations for describing several brain tumor areas in the MRI scans. Such descriptions are essential for researchers to train and quantify algorithms, employed for precisely identifying and classifying diverse kinds of BTs, like gliomas. Such a tumor further has several grades.

3.1.2. Glioma Dataset

This dataset is quite significant in detecting brain tumor as it contains information related to glial cells in the centre nervous system. The Cancer Genome Atlas (TCGA) Glioma Dataset is a complete storage source of molecular and medical information from an extensive unit of glioma patients. The TCGA was an extensive model, utilizes for unravelling the complicated genetic and epigenetic foundations of gliomas. Hence, these tumors and probable opportunities, for targeted treatments, are understood in depth. Besides, the Rembrandt data set is considered to attain genetic factor data and healthcare information, that leads to maximize the domain resources for glioma research. The research scholars and medicinal experts widely employed these datasets for attaining higher accuracy in diagnosis and cure approaches for gliomas, which enhance the patient care in neuro-oncology.

3.2. Methodology

This work projects a mechanism on the basis of TL which is an integrated mechanism of VGG16 and CNN to detect brain tumor. Fig. 1 demonstrates the procedure to diagnose BTs from MRI.

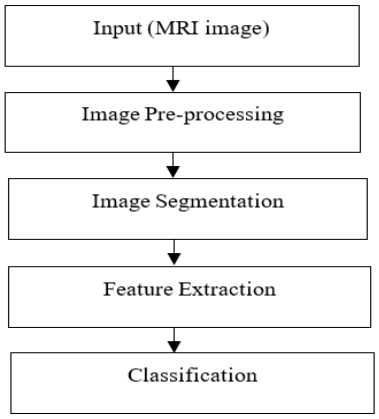

Fig 1. Images showing the visual symptoms cause by fungal disease

Distinct stages are executed for detecting brain tumor which are discussed below: -

1. Input MRI image and Pre-process: - In this, MRI scan is fed into the projected mechanism in input and Gaussian filter assists in pre-processing the images. This filter is effective to lessen noise and remove blurriness from the images. This filter is named as smoothing operator. Furthermore, it assists in eliminating details related to images that exists naturally. The impulse response is recognized as a Gaussian function. This function helps to highlight the probability to distribute noise and eliminate the Gaussian noise in a precise manner. This filter is performed non-uniformly, linearly and low pass on the basis of Gaussian function of a given SD.

2. Segmentation: - The snake segmentation scheme is taken into consideration to segment the brain area from Magnetic Resonance Imaging scan. This scheme is designed according to raster scan. Consequently, it has potential to cover extreme edges of picture. The SAC framework [6-8] assists in establishing a parameterized primary contour curve (CC) in picture space, and formulating an energy function (EF) to describe the shape of the region concerning internal energy (IE) and external energy (EE). The first one is determined relied on the attributes of curve. The concept of curvature, curve length, etc., is considered to allow the features of an image to explain the final power. The major intend is to alleviate the EF for converging the primary CC $C(s) = (x(s), y(s), s \in [0,1])$ at quick level towards the boundary of terminus area, considering both energies:

$$(C) = \int_0^1 \alpha E_{int}(C(s)) + E_{img}\left(C(s) + \gamma E_{con}(C(s))\right) ds \quad (1)$$

The given equation represents three sections in EF and E_{int} denotes IE for ensuring the smooth and regular nature of curve; E_{img} illustrates the image energy whose allocation is done with attributes of predicted place, such as edges; and the restricted power (curve) is shown with E_{con}. The fundamental emphasis is on determining the length and curvature. The SAC approach is implemented as it contains geometric constraints. In addition of image quality, this approach is effective to extract the smoother and fastened boundaries. Though, several issues are occurred. The complicated one is to tackle its dependency on the principal contour. The position, shape and number of control points attain potential to generate the required outcome when a suitable primary contour is selected.

3. Filtering: - Diverse types of noise lay impact on the Magnetic Resonance Imaging scans. This noise is eliminated using the PNLM method, an expanded form of NLP. This method is effective de-noise the images. In contrast to traditional scheme, this method works efficiently at smallest Mean Square Error value. An image has the weighted average of all the voxel concentrations and this method is also efficient to quantify the stored intensity value of the voxel. For a discrete noisy image, u = {u(i)|i∈ I}, this process aims to evaluate a predictive value of NL[u](i), for a pixel i, as a weighted average about every pixel available in image,

$$\text{NL[u] i} = \sum_{j \in I} W(i,j) u(j) \quad (2)$$

The resemblance among the pixels i and j is the base on which family of weights {w(i, j)}j depends and also satisfy the conditions 0≤w(i, j)≤ 1 and w(i, j) = 1.A square neighbourhood of set size is denoted by the u(N_k) and centred at a pixel k, while on the resemblance of the intensity Gray level vectors u(N_i) and u(N_j) is the base on which likeness of two pixels i and j relies. In order to compute the resemblance, the decreasing function of Euclidean distance is measured shown below:

$$\left\| u(N_i) - u\left(N_j\right) \right\|_2^2, a \quad (3)$$

Where, 'a' is specified as the standard deviation of the Gaussian kernel and is larger than zero. The application of the Euclidean distance to the noisy neighbourhoods raises the following equality:

$$\text{E}\left\| u(N_i) - u\left(N_j\right) \right\|_2^2, a = \left\| u(N_i) - u\left(N_j\right) \right\|_2^2, a + 2a^2 \quad (4)$$

The order of resemblance among pixels is maintained by the Euclidean distance and also this similarity depicts the

sturdiness of the algorithm. There is larger weight in the average of the pixels containing a analogous Gray level neighbourhood. These weights are defined as,

$$W(i, j) = \frac{1}{z(i)} e^{-\|u(N_i) - u(N_j)\|_{2,a}^2 / h^2} \quad (5)$$

Where Z (i) is the normalizing constant

$$Z(i) = \sum e^{-\|u(N_i) - u(N_j)\|_{2,a}^2 / h^2} \quad (6)$$

Where, parameter 'h' behaves as a degree of filtering. The regression of the exponential function is restricted by this parameter and the degree of filtering is represented by the parameter 'h'. The exponential function regression is controlled by this due to which regression of the weights is alike to a function of the Euclidean distances.

4. Classification: A TL model which is an integration of VGG16 and Convolutional Neural Network is implemented to categorize brain tumor. The first one is utilized as a basis system in which latter one helps to train data.

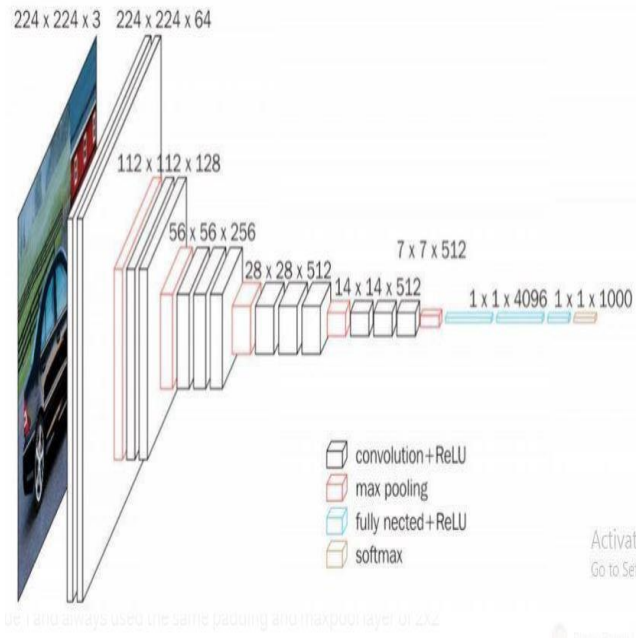

Fig 2. VGG16 Model Architecture

Different stages of VGG16 are defined as: -

1. This model has 16 to show 16 layers. The weights are assigned to every layer. In this, 13 layers are conv., 5 are MP, and 3 are Dense layers and 21 layers are available. Though, only 16 weight layers: learnable metrics layers, are taken in account.

2. The tensor size fed in input of this model is of 224, 244 having 3 RGB channel

3. Only small amount of hyper-parameters are deployed in this algorithm. Its conv. layers are deployed along with of 3x3 filter having stride 1, and similar padding and MP layer is of 2x2 filter of stride

4. The complete design of this technique help in arranging the conv. and MP layers at reliable level.

5. The Conv-1 Layer is composed of sixty-four filters, Conv-2 of 128, Conv-3 256, Conv 4 and Conv 5 layers of 512.

6. 3 FC is inserted with diverse Conv. layers. There are 4096 channels comprised in first 2 layers and the final one is assisted in executing 1000-way ILSVRC classification. Around 1000 channels are available in this layer. This layer is recognized as a soft-max layer.

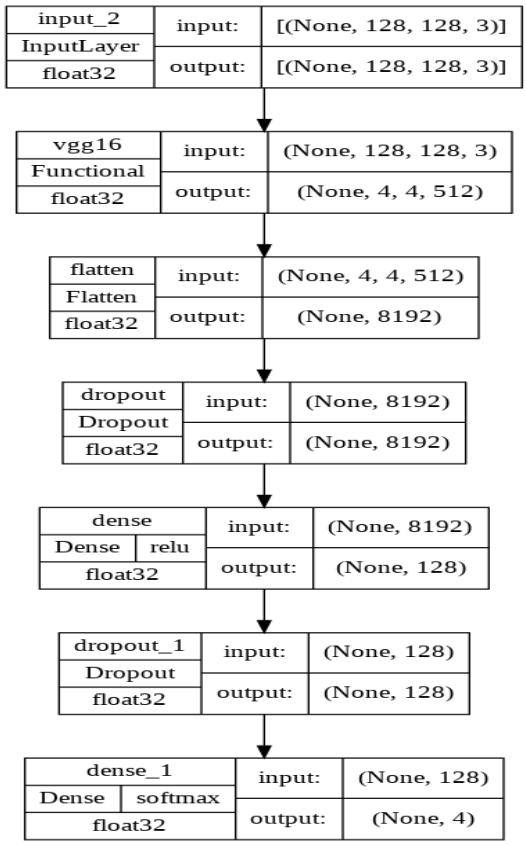

Fig 3. VGG16 Mode

4. Results and Discussion

This work employs a TL method to diagnose the brain tumor. A comprehensive assessment is performed on the projected approach against other deep learning (DL) and machine learning (ML) techniques. BRATS and Glioma datasets are applied for evaluating the efficacy of the projected approach with respect to accuracy, precision, recall, F1-score, and ROC.

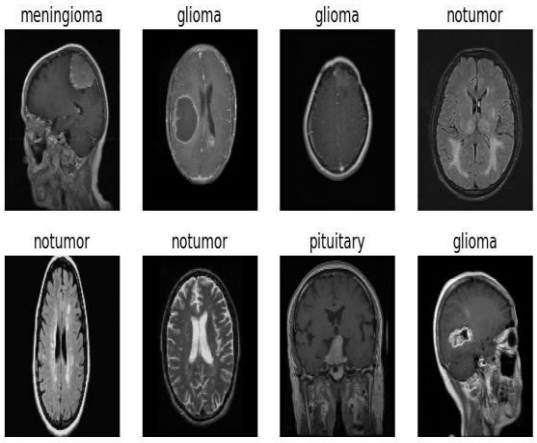

Fig. 4. Sample Images of Glioma dataset

Fig. 4 demonstrates the sample images taken from the Glioma dataset. Moreover, 4 distinct classes are shown in these images which are Meningioma, Glioma, No Tumor and Pituitary. Fig. 5 illustrates the share of every class in a percentage.

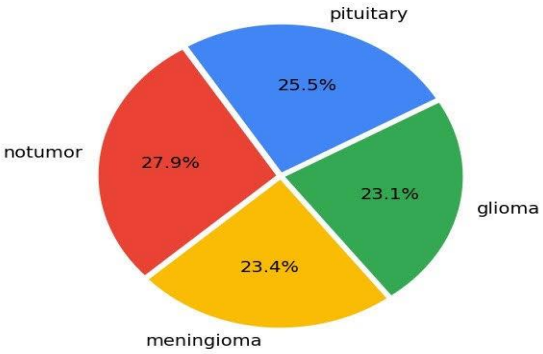

Fig. 5. Class Distribution

Table 1 demonstrates a complete overview of evaluation parameters of projected approach on the Glioma Dataset for numerous ML algorithms, namely Alexnet, VGG16, CNN, Random Forest, Support Vector Machine, and KNN.

Table 1. Model Performance of Glioma Dataset

Model	***Precision***	***Recall***	***Accuracy***	***F1-Score***
Alexnet	92.25	93.25	93.57	91.35
VGG16	93.27	93.72	95.23	94.22
CNN	92	91	91	91
Random Forest	54	64	66	57
Support Vector Machine	77	77	78	77
KNN	68	68	70	68

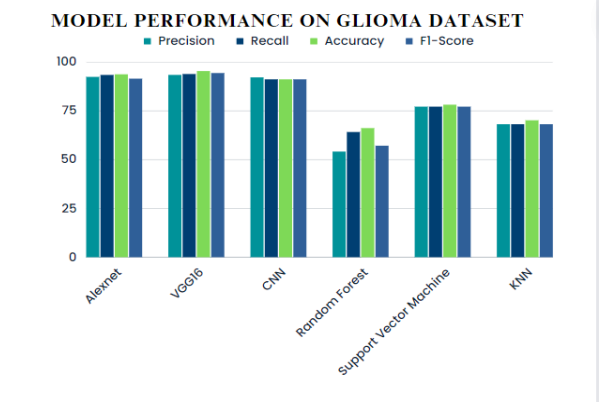

Fig.6. Performance Analysis on Glioma Dataset

Fig. 6 depicts the graphical illustration of efficiency of dissimilar DL and ML algorithms on the Glioma dataset to detect brain tumor. The precision, recall, accuracy, and F1-score are considered to quantify the potentials of these algorithms for classifying brain tumor cases in an accurate way. AlexNet leads to recognize a major portion of true positive (TPs) cases among its positive predictions at 0.9225 precision with a recall of 0.9325, that implied it assists in capturing an enormous size of actual positive samples. Thus, the accuracy is obtained up to 0.9357 and an F1-score around 0.9135, which depicts a balance amid precision and recall. Further, the precision of VGG16 algorithm is found 0.932, recall is 0.937, accuracy is 0.952 andF1-score is 0.9422. Hence, this algorithm is proved robust for categorizing tumorous images. Meanwhile, CNN and RF algorithm offer higher accuracy up to 0.91. But, their precision and recall are changed. The SVM is performed effectively for recognizing tumorous area at precision and recall of 0.77 and accuracy of 0.78. This technique is robust to handle the task related to classify tumors successfully. In the end, KNN algorithm provides a moderate precision up to 0.68, recall around 0.68 and accuracy up to 0.70, and proved effective to detect tumor.

Table 1. Model Performance of BRATS Dataset

Model	***Precision***	***Recall***	***Accuracy***	***F1-Score***
Alexnet	88.43	87.9	88.67	87.65
VGG16	93.32	93.67	94.54	94.21
CNN	76	76	76	76
Random Forest	77	69	75	71

Support Vector Machine	75	67	73	67
KNN	61	61	63	61

Table 2 demonstrates the efficiency of the projected approach with respect to diverse parameters on BRATS dataset, such as precision, recall, accuracy, and F1-Score, for diverse machine learning (ML) algorithms.

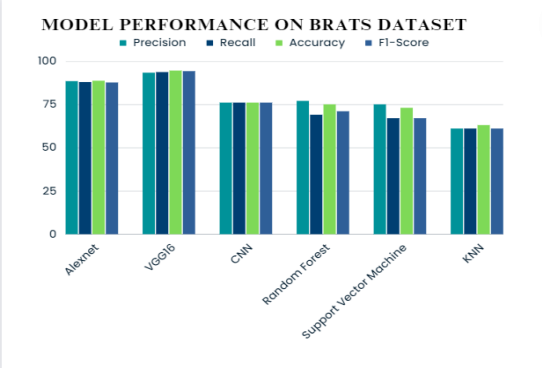

Fig.7. Performance Analysis on BRATS Dataset

Figure 7 illustrates the evaluation of diverse DL and ML method on BRATS dataset to detect brain tumor and offered results on the basis of accuracy, precision, and recall. These measures assist in analysing the given approaches to classify brain tumor and their potentials to lessen FPs and FNs. AlexNet is employed to recognize a specific portion of TPs among positive forecasting and detect tumor at precision of 0.8843 and recall of 0.879 after capturing a wide region of real time tumorous samples. This algorithm offered an accuracy of 0.8867 and an F1-Score up to 0.8765. Hence, it proved that this algorithm is more stable and balances the precision and recall. VGG16 works well in detecting infected images at precision of 0.9332, recall of 0.9367, accuracy of 0.9454 and an F1-Score up to 0.9421. It aids in categorizing the samples and diminishing FPs and FNs. CNN algorithm provides a precision, recall and accuracy of 0.76 each while classifying tumorous samples precisely. The RF model leads to detect tumor at precision of 0.77 and recall of 0.69 which enhances the accuracy around 0.75. Though, the accuracy of this algorithm is superior yet its precision and recall is changed to provide trade-off among these parameters. Likewise, SVM method attains 0.75 precision, 0.67 recall which leads to provide 0.73 accuracy. Consequently, the applicability of this method is exhibited to categorize brain tumor samples but provides some false negatives (FNs). At last, the precision and recall of K-Nearest Neighbors (KNN) algorithm are found 0.61 each, and its accuracy is found 0.63. This algorithm results in striking a balance amid TPs and TNs. However, it is ineffective to augment precision or recall.

5. Conclusion

It is summarized that the Glioma and BRAT datasets are exploited to quantify the DL and ML algorithms to recognize brain tumor. It is analysed that the various algorithms are consistent to enhance the value of diverse measures. The effectiveness of VGG16 approach is exhibited to provide exceptional accuracy, precision, recall, and F1-Score. According to results on Glioma dataset, this approach is robust for detecting brain tumor at 0.9327 precision, 0.9372 recall, 0.9523 accuracy, and 0.9422 F1-Score. Henceforth, this approach is worked effectively to classify the images after capturing the real time samples. The results on this dataset demonstrates the supremacy of this approach over other algorithms. According to results on BRAT dataset, the projected approach detected the brain tumor at 0.9332 precision, 0.9367 recall, 0.9454 accuracy, and 0.9421 F1-Score. Moreover, this approach is quite feasible to detect BT concerning all the measures. Moreover, this approach was accurate and consistent to categorize BT. To conclude, the projected approach worked more robustly in contrast to other techniques on both data sets for rendering superior values for all metrics. Consequently, this algorithm is presented as an effectual mechanism to diagnose BT. Furthermore, to classify medical imaging, the VGG16 is proved robust and reliable for maintaining higher accuracy in comparison with other metrics. It is considered as precise tool for doctors to diagnose BTs in an accurate way prior to provide care and treatment on time.

References

[1] L. Brunese, F. Mercaldo, A. Reginelli and A. Santone, "Neural Networks for Lung Cancer Detection through Radiomic Features," 2019 International Joint Conference on Neural Networks (IJCNN), 2019, pp. 1-10

[2] P. Lobo and S. Guruprasad, "Classification and Segmentation Techniques for Detection of Lung Cancer from CT Images," 2018 International Conference on Inventive Research in Computing Applications (ICIRCA), 2018, pp. 1014-1019

[3] S. S. Raoof, M. A. Jabbar and S. A. Fathima, "Lung Cancer Prediction using Machine Learning: A Comprehensive Approach," 2020 2nd International Conference on Innovative Mechanisms for Industry Applications (ICIMIA), 2020, pp. 108-115

[4] J. B. S. Carvalho, J. -M. Moreira, M. A. T. Figueiredo and N. Papanikolaou, "Automatic Detection and Segmentation of Lung Lesions using Deep Residual CNNs," 2019 IEEE 19th International Conference on Bioinformatics and Bioengineering (BIBE), 2019, pp. 977-983

[5] K. Suzuki, "Small Data Deep Learning for Lung Cancer Detection in CT," 2022 IEEE Eighth International Conference on Big Data Computing Service and Applications (BigDataService), 2022, pp. 114-118

[6] A. R. S. Soares, T. J. B. Lima, R. d. A. L. Rabêlo, J. J. P. C. Rodrigues and F. H. D. Araujo, "Automatic Segmentation of Lung Nodules in CT Images Using Deep Learning," 2020 IEEE International Conference on E-health Networking, Application & Services (HEALTHCOM), 2021, pp. 1-6

[7] H. Mahersia, H. Boulehmi and K. Hamrouni, "CAD system for lung nodules detection using wavelet-based approach and intelligent classifiers," 2020 17th International Multi-Conference on Systems, Signals & Devices (SSD), 2020, pp. 173-178

[8] A. Shaffie et al., "A New System for Lung Cancer Diagnosis based on the Integration of Global and Local CT Features," 2019 IEEE International Conference on Imaging Systems and Techniques (IST), 2019, pp. 1-6

[9] W. M. Salama and M. H. Aly, "Lung CT Image Segmentation: A Generalized Framework Based on U-Net Architecture and Pre-processing Models," 2021 31st International Conference on Computer Theory and Applications (ICCTA), 2021, pp. 141-146

[10] B. Bahat and P. Görgel, "Lung Cancer Diagnosis via Gabor Filters and Convolutional Neural Networks," 2021 Innovations in Intelligent Systems and Applications Conference (ASYU), 2021, pp. 1-6

[11] J. Cañada, E. Cuello, L. Téllez, J. M. García, F. J. Velasco and J. Cabrera, "Assistance to lung cancer detection on histological images using Convolutional Neural Networks," 2022 E-Health and Bioengineering Conference (EHB), 2022, pp. 1-4,

[12] S. K. Gautam, S. Pandey, S. K. Sinha and Kirti, "Graphical User Interface based platform for the Lung Cancer Classification," 2022 International Conference on Emerging Smart Computing and Informatics (ESCI), 2022, pp. 1-5

[13] S. Das and S. Majumder, "Lung Cancer Detection Using Deep Learning Network: A Comparative Analysis," 2020 Fifth International Conference on Research in Computational Intelligence and Communication Networks (ICRCICN), 2020, pp. 30-35

[14] A. Masood et al., "Cloud-Based Automated Clinical Decision Support System for Detection and Diagnosis of Lung Cancer in Chest CT," in IEEE Journal of Translational Engineering in Health and Medicine, vol. 8, pp. 1-13, 2020

[15] Gupta, S., Chhabra, A., Agrawal, S., Singh, S.K. A Comprehensive Comparative Study of Machine Learning Classifiers for Spam Filtering. In: Nedjah, N., Martínez Pérez, G., Gupta, B.B. (eds) International Conference on Cyber Security, Privacy and Networking (ICSPN 2022). Lecture Notes in Networks and Systems, vol 599. Springer, 2023.

[16] Verma, R., Chhabra, A., & Gupta, A. A statistical analysis of tweets on COVID-19 vaccine hesitancy utilizing opinion mining: an Indian perspective. Social Network Analysis and Mining, 13(1), 12. Springer Vienna, 2022

[17] N. Maleki and S. T. AkhavanNiaki, "An intelligent algorithm for lung cancer diagnosis using extracted features from Computerized Tomography images", Healthcare Analytics, vol. 14, no. 3, pp. 517-529, 27 February 2023

[18] D. Rammurthy and P. K. Mahesh, "Whale Harris Hawks optimization based deep learning classifier for brain tumor detection using MRI images", Journal of King Saud University - Computer and Information Sciences, vol. 51, no. 12, pp. 5859-5870, 15 August 2020

[19] E. Dandıl and S. Karaca, "Detection of pseudo brain tumors via stacked LSTM neural networks using MR spectroscopy signals", Biocybernetics and Biomedical Engineering, vol. 41, no. 5, pp. 173-195, 30 December 2020

[20] Shiny, K. V., and N. Sugitha. "Effective Brain Tumor Classification on MRI Using Deep Belief-convolutional Neural Network with Pixel Change Detection based on Pixel Mapping Technique." Technology 2021

[21] R. Vankdothu and M. A. Hameed, "Brain tumor MRI images identification and classification based on the recurrent convolutional neural network", Measurement: Sensors, vol. 7, pp. 131270-131281, 23 August 2022

[22] Okashi, Omar Munthir Al, and Ismail Taha Ahmed. "Brain tumor detection based on multiple features." In AIP Conference Proceedings, vol. 2400, no. 1, p. 020011. AIP Publishing LLC, 2022.

[23] Senan, Ebrahim Mohammed, Mukti E. Jadhav, Taha H. Rassem, Abdulaziz SalamahAljaloud, BadieaAbdulkarem Mohammed, and ZeyadGhaleb Al-Mekhlafi. "Early diagnosis of brain tumor MRI images using hybrid techniques between deep and machine learning." Computational and Mathematical Methods in Medicine 2022

[24] Raza, Rehan, Usama Ijaz Bajwa, Yasar Mehmood, Muhammad Waqas Anwar, and M. Hassan Jamal.

"dResU-Net: 3D deep residual U-Net based brain tumor segmentation from multimodal MRI." Biomedical Signal Processing and Control 79, 103861, 2023

[25] Chang, Yankang, Zhouzhou Zheng, Yingwei Sun, Mengmeng Zhao, Yao Lu, and Yan Zhang. "Dpafnet: A residual dual-path attention-fusion convolutional neural network for multimodal brain tumor segmentation." Biomedical Signal Processing and Control 79, 104037, 2023

[26] Cao, Yuan, Weifeng Zhou, Min Zang, Dianlong An, Yan Feng, and Bin Yu. "MBANet: A 3D convolutional neural network with multi-branch attention for brain tumor segmentation from MRI images." Biomedical Signal Processing and Control 80, 104296, 2023

[27] S. Tripathy, R. Singh and M. Ray, “Automation of Brain Tumor Identification using EfficientNet on Magnetic Resonance Images”, Procedia Computer Science, vol. 2018, pp. 1551-1560, 31 January 2023